MAP-based sparse detection strategies. Application to the hyperspectral data of the MUSE instrument.

Silvia Paris, David Mary, André Ferrari

Laboratoire Lagrange, UMR7293,
Université de Nice Sophia-Antipolis, CNRS, Observatoire de la Côte d'Azur,
Campus Valrose, 06108 Nice - cedex 02, FRANCE

Email: {Silvia.Paris, David.Mary, Andre.Ferrari}@unice.fr

Abstract

Recent works showed efficient and reliable detection techniques for the analysis of the astrophysical hyperspectral data of the MUSE (Multi Unit Spectroscopic Explorer) instrument. In particular, two composite detection tests based on Maximum A Posteriori (MAP) estimates were shown to be more powerful than the Generalized Likelihood Ratio (GLR) test in the case of sparse parameters. These tests are the Posterior Density Ratio (PDR), which computes the ratio of the a posteriori distribution under each hypothesis, and the LRMAP, where the MAP replaces the Maximum Likelihood estimate. After summarizing the theoretical properties of the considered sparse detection tests, we turn to detection strategies that take into account not only the spectral but also the spatial dependencies that exist between neighbor spectra in the data cube. In this contribution, we propose an analysis of the resulting global False Alarm rate (FA) for each given spectra, through the use of FA-maps. Numerical comparisons are presented on simulated data cubes provided by the MUSE consortium.

I. Introduction

The ESO VLT instrument MUSE is a second generation integral field spectrograph, which will provide a huge quantity of hyperspectral data composed by cubes of 300×300 spectra sampled at ≈ 4000 wavelengths of the visible spectrum. The expected performances of MUSE should allow the detection of very distant galaxies, seen at more than 10 billions light-years distance. One of the challenging scientific objectives is then the detection and the characterization of extremely faint and tiny astrophysical sources. Such light sources are spatially localized within very few pixels and may show only a few spectrally salient features. The processing of such data therefore poses important challenges. First, the data will be acquired at very low signal-to-noise ratio with a highly variable noise level, which strongly depends on the spectral and spatial coordinates in the data cube. Second, the size of the data calls for estimation and detection methods that cannot be arbitrarily complex.

In this context, we have proposed in recent works efficient and reliable *detection* techniques for the analysis of MUSE data based on the use of composite hypothesis tests, which are adapted to sparse signals through the use of MAP estimates. Methods based on sparse representations are indeed particularly appropriate for such data as they operate a reduction of the dimension, while preserving accurate data modeling. The two detection tests we consider are the PDR (introduced by Basu in 1996 [2] but not in the context of sparse signals) and the LRMAP tests, which showed better performances than classical tests (i.e. Generalized Likelihood Ratio Test and Bayes Factor [10]) for hyperspectral data.

The definitions of the tests and a comparison of their performances for a first simple introducing model, are reported in Sec.II. A more realistic model is considered in Sec.III, for which the tests are set up in order to take advantage of a specific redundant dictionary, especially designed for MUSE spectra in accordance with astrophysical knowledge. An analysis of the reliability of the tests, based on the computation of the $P-$value for all spectra in the data cube, is proposed. The tests are then applied to the detection of faint sources in MUSE hyperspectral data (Sec.IV). The observation model considered for MUSE spectra is reported in Sec.IV-A. According to this model, the detection performances of the tests are increased by exploiting not only the spectral but also the spatial dependences existing between spectra in the data cube. In this context, a subsequent analysis of the reliability of the tests, based on the computation of the overall FA rate for each spectrum and illustrated through the use of FA maps, is proposed in Sec.IV-B, before concluding the paper.

II. Detection Tests

We first consider the following introductory model:

$$\begin{cases} \mathcal{H}_0 : \boldsymbol{x} = \boldsymbol{\epsilon}, & \boldsymbol{\epsilon} \sim \mathcal{N}(0, \Sigma) \\ \mathcal{H}_1 : \boldsymbol{x} = \boldsymbol{\theta} + \boldsymbol{\epsilon} \end{cases} \tag{1}$$

where $\boldsymbol{x}, \boldsymbol{\theta}$ and $\boldsymbol{\epsilon}$ are real N-vectors and $\boldsymbol{\theta}$ is an unknown deterministic vector of parameters with few nonzero components. Given the two hypotheses of the model, a detection test generally reduces to compute

$$T(\boldsymbol{x}) \underset{H_0}{\overset{H_1}{\gtrless}} \gamma, \tag{2}$$

where the test statistic $T(\boldsymbol{x})$ is compared to a test threshold γ which permits to control the probability of false alarm (P_{FA}) of the test, defined as $P_{FA}(\gamma) = Pr(T(\boldsymbol{x}) > \gamma; \mathcal{H}_0)$.

The detection tests we compare are:

- the Generalized Likelihood Ratio test [7]

$$T_{GLR}(\boldsymbol{x}) = \frac{\max\limits_{\boldsymbol{\theta}} p\left(\boldsymbol{x} \mid \boldsymbol{\theta}\right)}{p\left(\boldsymbol{x} \mid \mathbf{0}\right)}; \tag{3}$$

- the Posterior Density Ratio test

$$T_{PDR}(\boldsymbol{x}) = \frac{\max\limits_{\boldsymbol{\theta}} p\left(\boldsymbol{\theta} \mid \boldsymbol{x}\right)}{p\left(\mathbf{0} \mid \boldsymbol{x}\right)}; \tag{4}$$

- a Likelihood Ratio test in which $\boldsymbol{\theta}$ is replaced by its MAP estimate:

$$T_{LRMAP}(\boldsymbol{x}) = \frac{p\left(\boldsymbol{x} \mid \hat{\boldsymbol{\theta}}_{MAP}\right)}{p\left(\boldsymbol{x} \mid \mathbf{0}\right)}, \tag{5}$$

  where $\hat{\boldsymbol{\theta}}_{MAP} = \arg\max\limits_{\boldsymbol{\theta}} p\left(\boldsymbol{x} \mid \boldsymbol{\theta}\right) \pi\left(\boldsymbol{\theta}\right)$ and $\pi(\boldsymbol{\theta})$ denotes a Laplacian prior probability distribution of the form

$$\pi(\boldsymbol{\theta}) = \prod_{i=i}^{N} \frac{1}{2\lambda_i} e^{-\frac{|\theta_i|}{\lambda_i}}. \tag{6}$$

This distribution allows a simple analytical computation of the MAP estimate, and is particularly appropriate for the detection of sparse parameters, as it leads to solutions ($\hat{\boldsymbol{\theta}}_{MAP}$) in which 0 values are favored.

The GLR test definition given in eq.(3) leads, after some computation, to [7]:

$$T_{GLR}(\boldsymbol{x}) = \sum_{i=1}^{N} \frac{x_i^2}{\sigma_i^2}.$$

Noting $\Sigma^{-\frac{1}{2}}\boldsymbol{x} = \boldsymbol{u}$ the vector of data weighted by the noise levels, we obtain

$$T_{GLR}(\boldsymbol{u}) = \|\boldsymbol{u}\|_2^2. \tag{7}$$

For the PDR test, the definition in (4) using a Laplacian prior leads to

$$T_{PDR}(\boldsymbol{u}) = \sum_{i=1}^{N} (|u_i| - \eta_i)^2 I(|u_i| > \eta_i), \tag{8}$$

where $I(\cdot)$ represents the indicator function and $\eta_i = \frac{\sigma_i}{\lambda_i}$. Finally, the LRMAP test in (5) gives

$$T_{LRMAP}(\boldsymbol{u}) = \sum_{i=1}^{N} (u_i^2 - \eta_i^2) I(|u_i| > \eta_i). \tag{9}$$

For model (1) with Laplacian prior, the MAP estimate corresponds to a soft-thresholding of each u_i at thresholds η_i [8]. In order to set the same FA rate on each component, the η_i should be made equal to some value, say η.

The PDR and LRMAP tests, of the general form in (2), depend on both the η and γ parameters (see [9], for further details). The maximal FA rate for a fixed η (P_{FA_0}) is thus obtained by setting $\gamma = 0$:

$$\begin{aligned} P_{FA_0} = Pr(T > 0 | \mathcal{H}_0) &= 1 - Pr(|u_i| < \eta \; \forall i) \\ &= 1 - (2\Phi(\eta) - 1)^N. \end{aligned} \tag{10}$$

This allows to precisely fix the probability of false alarm by tuning the sole η threshold. In a similar way, the probability of detection for $\gamma = 0$ is expressed as:

$$P_{DET_0}(\boldsymbol{\theta}) = 1 - \prod_{i=1}^{N} [\Phi(\eta - \theta_i) + \Phi(\eta + \theta_i) - 1]. \tag{11}$$

Fig.1 shows the ROC curves of the PDR, LRMAP and GLR tests, plotted considering a $N = 400$ component vector $\boldsymbol{\theta}$ of which only 10 are different from zero, with linearly increasing values in $[0.5; 5]$, for $\eta = 3.7$ (dashed lines) and 4.2 (continuous lines). Since η is fixed in each figure, different values of P_{FA} are obtained by varying γ. The Oracle test, for which the support of $\boldsymbol{\theta}$ is known, is here reported as a further reference (in cyan). While always outperforming the GLR test, the LRMAP and the PDR performances generally differ, in line with the considered values of the η threshold. Consequently, different values

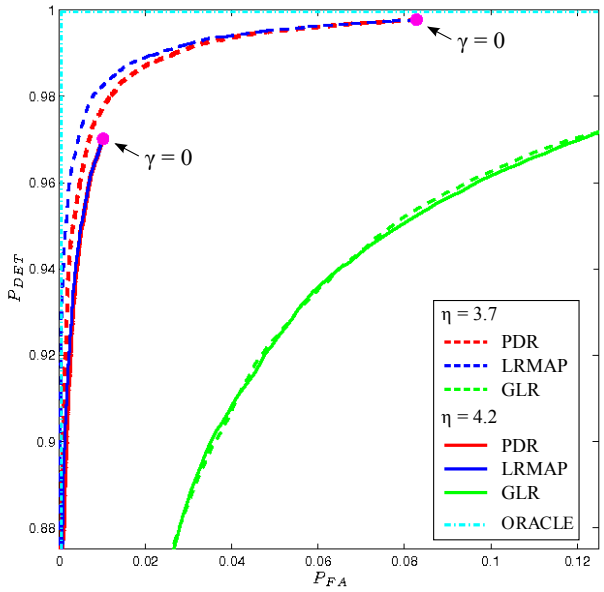

Fig. 1. PDR (in red), LRMAP (in blue) and GLR (in green) ROC curves for $\eta = 3.7$ (dashed lines) and $\eta = 4.2$, considering a $N = 400$ component vector $\boldsymbol{\theta}$ of which only 10 are different from zero, with linearly increasing values in $[0.5; 5]$. The Oracle test, for which the support of $\boldsymbol{\theta}$ is known, is reported (in cyan) as a reference. Magenta points correspond to the maximal probability of false alarm and probability of detection at a given η. The coordinates of those points are written in closed form in eq. (10) and (11).

of P_{FA_0} and P_{DET_0} are reached for different η. These values correspond to the coordinates of the two magenta points in the figure. Since both T_{PDR} and T_{LRMAP} tests statistics are positive (see eq.(8) and (9)), in these points the two detection tests are equivalent and detection is claimed as soon as at least one weighted component $|u_i|$ is larger than η. To keep the tests simple, we will focus on the $\gamma = 0$ case, for which satisfactory detection performances can be achieved even for more general and realistic models, as presented in the following sections.

III. Model based on a redundant dictionary

In this section we turn to a more realistic model in which sparsity is promoted through the use of a redundant dictionary [10]:

$$\begin{cases} \mathcal{H}_0 : \boldsymbol{x} = \boldsymbol{w}, \qquad \boldsymbol{w} \sim \mathcal{N}(\mathbf{0}, I) \\ \mathcal{H}_1 : \boldsymbol{x} = D\boldsymbol{\theta} + \boldsymbol{w} \end{cases} \tag{12}$$

where $D = [\boldsymbol{D}_1 \dots \boldsymbol{D}_L]$ is a redundant normalized dictionary of size $(N \times L)$ with $L > N$ atoms and $\boldsymbol{\theta}$ is a column vector of L components, assumed to be sparse. For the PDR and the LRMAP tests, still considered for a Laplacian prior law, the $\hat{\boldsymbol{\theta}}_{MAP}$ estimate is in this case the solution of the Basis Pursuit Denoising (BPDN) [4] expression:

$$\hat{\boldsymbol{\theta}}_{MAP} = \arg\min_{\boldsymbol{\theta}} \frac{1}{2} \|\boldsymbol{x} - D\boldsymbol{\theta}\|^2 + \eta \|\boldsymbol{\theta}\|_1 . \tag{13}$$

According to this and to the definitions of the tests given in Sec.II, the computation of the tests statistics for model (12) yields to [10]:

$$T_{PDR}(\boldsymbol{x}) \underset{H_0}{\overset{H_1}{\gtrless}} \gamma \Leftrightarrow \frac{1}{2} \hat{\boldsymbol{x}}^t_{MAP} \hat{\boldsymbol{x}}_{MAP} \underset{H_0}{\overset{H_1}{\gtrless}} \gamma \tag{14}$$

$$T_{LRMAP}(\boldsymbol{x}) \underset{H_0}{\overset{H_1}{\gtrless}} \gamma \Leftrightarrow \eta \left\| \hat{\boldsymbol{\theta}}_{MAP} \right\|_1 + \frac{1}{2} \hat{\boldsymbol{x}}^t_{MAP} \hat{\boldsymbol{x}}_{MAP} \underset{H_0}{\overset{H_1}{\gtrless}} \gamma, \tag{15}$$

where $\hat{\boldsymbol{x}}_{MAP} = D\hat{\boldsymbol{\theta}}_{MAP}$. From these expressions we see that both test statistics are strictly positive, or null if and only if $\hat{\boldsymbol{\theta}}_{MAP} = \mathbf{0}$ (that is, if $\max_i(|\boldsymbol{D}_i{}^t \boldsymbol{x}|) \leq \eta$). Similarly to Sec.II, the maximal P_{FA} considering both tests at $\gamma = 0$ is given by

$$\begin{aligned} P_{FA_0} &= Pr(T > 0 \mid \mathcal{H}_0) \\ &= Pr(\max_i(|\boldsymbol{D}_i{}^t \boldsymbol{x}|) > \eta \mid \mathcal{H}_0). \end{aligned} \tag{16}$$

As the two tests are strictly equivalent at $\gamma = 0$, from now on we will refer to this unique test as the PDR/LRMAP test.

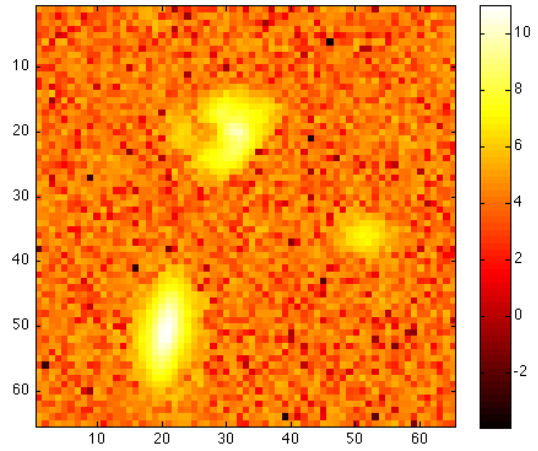

(a) Log scaled version of the considered noisy MUSE sub-cube

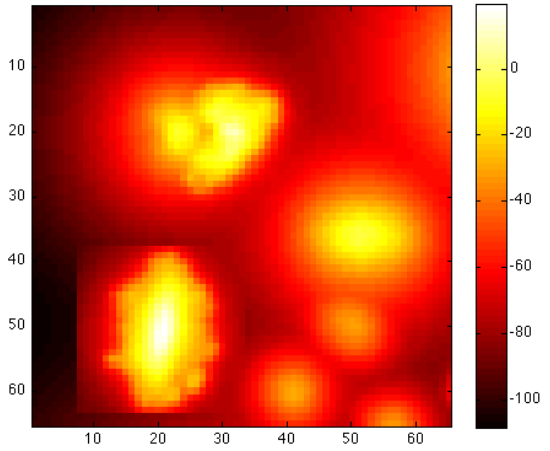

(b) SNR map

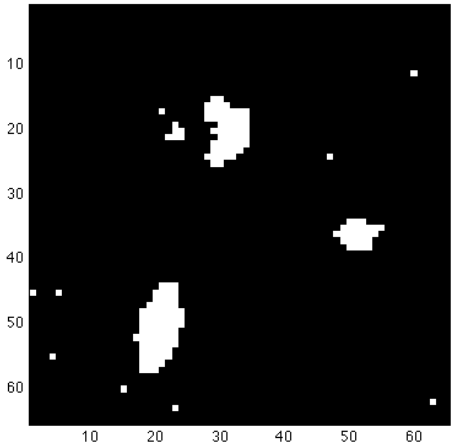

(c) Detection results using the GLR test (168 detections)

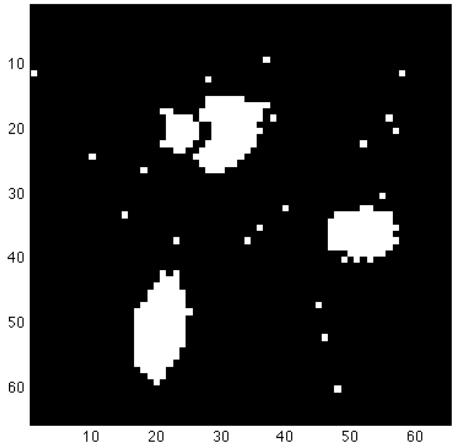

(d) Detection results using the PDR/LRMAP test (315 detections)

Fig. 2. Compared detection performances of PDR/LRMAP and GLR tests on a MUSE sub-cube, for a same $P_{FA} = 0.002$.

Note that, since D is redundant, the components of the L-vector $D^t\boldsymbol{x}$ are not independent, and finding P_{FA_0} analytically is thus a difficult problem (see [6]). We can nevertheless resort to Monte Carlo (MC) simulations to obtain an accurate correspondence between η and P_{FA_0} [10]. For instance, for the dictionaries considered below, a P_{FA_0} of 0.002 is typically obtained with $\eta = 5.2$.

Note finally that for $\gamma = 0$, it is not necessary to solve (13) to implement these detection tests, as they both amount to compare $\max_i(|\boldsymbol{D}_i{}^t\boldsymbol{x}|)$ to η. This test is not new in the literature and corresponds to the test used in [6]. This test is also called the *Max* test in [5] and [1]. While less performant for the detection of low sparsity level signals, the *Max* test showed to be optimal in [1], with respect to the Bayes risk, in the case of high sparsity levels. This result positively confirms the validity of our approach, specifically built for the detection of signals characterized by very few atoms in the dictionary D.

Fig. 2 shows the detection results obtained performing the GLR and the PDR/LRMAP tests on a MUSE simulated sub-cube. A log-scaled version of the considered noisy cube (sum over all wavelengths) is represented in Fig. 2(a). The correspondent SNR map is reported in Fig. 2(b) as a reference, to outline where exactly the objects of interest are located. For a same $P_{FA} = 0.002$, an increased number of detections is obtained using the PDR/LRMAP test. In particular, 168 detections are obtained with the GLR test (Fig.2(c)) and 315 detections with the PDR/LRMAP test (Fig.2(d)), thanks to the use of the adapted redundant dictionary and the injection of the MAP estimate in the tests.

To highlight the reliability of the detection results obtained with the PDR/LRMAP test, an analysis of the $P-$values, for all the spectra in the data-cube, is proposed hereafter. Defined as

$$P - \text{value} = Pr(\max_i(|\boldsymbol{D}_i{}^t\boldsymbol{x}| > t_{obs} \mid \mathcal{H}_0), \tag{17}$$

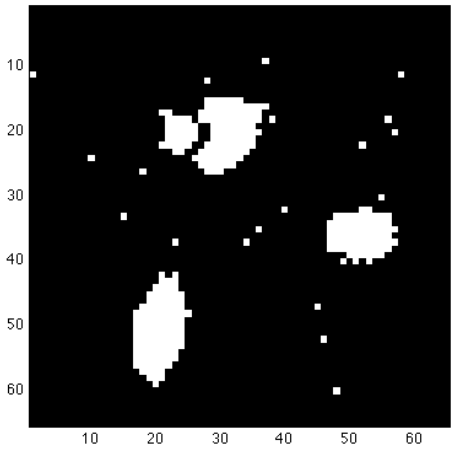

(a) Reference: detection map using PDR/LRMAP test with $P_{FA} = 0.002$

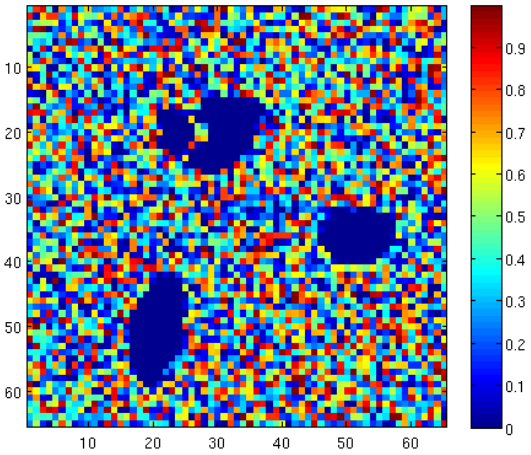

(b) $P-$value map computed for all the spectra in the sub-cube

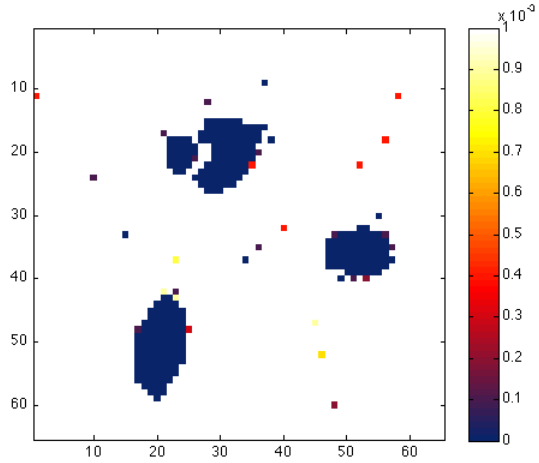

(c) $P-$value map thresholded at significance level $\alpha = 10^{-3}$

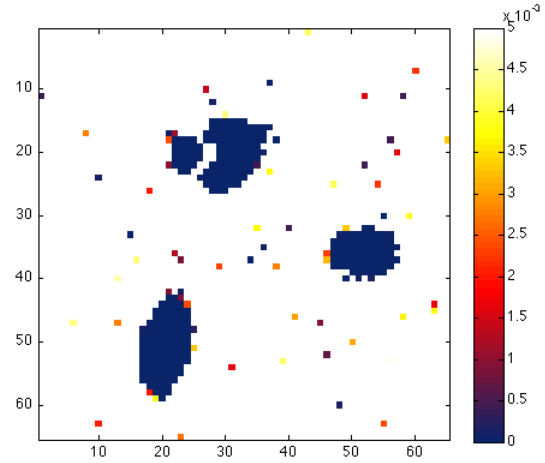

(d) $P-$value map thresholded at significance level $\alpha = 5 \cdot 10^{-3}$

Fig. 3. Comparison of the $P-$value maps computed for all spectra in the considered MUSE sub-cube at different values of the significance level α.

the $P-$value corresponds to the probability of obtaining, under the null hypothesis, a test statistic at least as extreme as the one that was actually observed (in this case, $t_{obs} = \max_i |\boldsymbol{D}_i{}^t \boldsymbol{x}_{obs}|$, where $\boldsymbol{x}_{obs}$ is a considered spectrum in the cube). When the $P-$value is less than a significance level α (generally $\alpha = 0.05$ or $\alpha = 0.01$), the result is said to be statistically significant.

Fig.3 compares different $P-$value maps computed for all the spectra in the MUSE sub-cube of Fig.2. In particular Fig.3(b) reports the $P-$value rates for each spectrum of the cube. Now, choosing an appropriate significance level α, and keeping in the map only pixels for which $P-$value $< \alpha$, we interestingly see that, despite few false alarms, pixels previously detected with the PDR/LRMAP test (reference in Fig.3(a)) are actually those characterized by lower $P-$values. Fig.3(c) and Fig.3(d) show the results respectively obtained choosing $\alpha = 10^{-3}$ and $\alpha = 5 \cdot 10^{-3}$. This proves statistical significance for most of the detections reached with the proposed test.

IV. Application to MUSE hyperspectral data

We finally apply the considered detection tests to astrophysical spectra restoration for the forthcoming MUSE instrument. MUSE is an integral-field spectrograph, which will be installed at the Very Large Telescope (ESO, Chile) at the end of 2012 and will deliver data cubes composed of 300×300 spectra sampled at ≈ 3600 wavelengths of the visible spectrum. One of the major challenges of MUSE concerns the detection and characterization of very distant galaxies. Such light sources are very faint, spatially localized within a few pixels and may show only a few spectrally salient features. Data will be acquired with very low signal-to-noise ratio. In particular, data will be strongly contaminated by the spectral signature of atmospheric molecules. In addition, data will be affected by a strong Poisson noise, which is indeed data dependent. Moreover, the instrumental detection efficiency is variable with wavelength. Consequently, the noise level is highly variable from one wavelength to another, and

also from one spectrum to another. This has consequences on the setting of the detection test, which will be made appearent in Sec. IV-A.

Considered as a linear system, MUSE is characterized by its three-dimensional point spread function (PSF, the impulse response in both spatial and spectral domains), that can be separated into the spatial PSF, which typically covers 7×7 pixels, and the spectral line spread function (LSF), which spreads over 11 spectral elements. Note that MUSE is still under construction, so only simulated data are available until now. These data result from high-complexity astrophysical simulations, and account for noise and instrument characteristics.

Restoration of MUSE-like spectra was recently addressed in [3], where prior information was incorporated through sparsity constraints. A redundant dictionary R of elementary spectral features was built in accordance with astrophysical knowledge, so that the sparsely estimated non-zero components can be interpreted as physically meaningful features. More precisely, R concatenates three sub-dictionaries : $R = [R^\ell\, R^c\, R^b]$, each of which corresponds to a specific spectral component: a line spectrum, a continuous spectrum and a series of discontinuities. R^ℓ is a dictionary of discrete splines with several widths, which are centered along the reconstruction wavelength axis. Eleven width values were used, varying from 1 (delta functions) to 138 points. Delta functions and splines model respectively unresolved and resolved absorption or emission spectral lines. MUSE' spectral resolution equals 0.13 nm so that the maximal width equals $138 \times 0.13 \simeq 18$ nm. The continuous spectrum is composed of sine functions with low frequencies (reduced frequencies vary from $1/N$ to $8/N$, where N is the number of data) and 8 discretized phase shifts. It also includes the continuous component by means of a constant signal. Finally, dictionary R^b models a series of breaks in the spectrum, and is composed of step functions which are also centered along the wavelength axis. While the works [3] used this dictionary in the framework of spectral restoration, we use it for detection purpose here. In the following, after formulating MUSE spectra as spatially independent, we consider a strategy to exploit spatial dependencies for which we suggest a way to analyse the overall FA rate, for each spectrum in the data cube.

A. The observation model

The observation model considered for MUSE spectra is [10]

$$\begin{cases} \mathcal{H}_0 : \boldsymbol{y} = \boldsymbol{\epsilon}, \\ \mathcal{H}_1 : \boldsymbol{y} = H\boldsymbol{s} + \boldsymbol{\epsilon} = HR\boldsymbol{\alpha} + \boldsymbol{\epsilon} \end{cases} \tag{18}$$

where H is the $(N \times N)$ matrix form of the LSF, R is $(N \times L)$, $\boldsymbol{\alpha}$ is a sparse L-vector and $\boldsymbol{\epsilon} \sim \mathcal{N}(\mathbf{0}, \Sigma)$ with $\Sigma = \text{diag}\{\sigma_1^2, \ldots, \sigma_N^2\}$. This model can be written as

$$\mathcal{H}_1 : \Sigma^{-\frac{1}{2}}\boldsymbol{y} = \Sigma^{-\frac{1}{2}}HR\boldsymbol{\alpha} + \boldsymbol{w}, \tag{19}$$

where $\Sigma^{-\frac{1}{2}}HR = D_{\Sigma H}$ appears as an equivalent dictionary, and $\boldsymbol{w} \sim \mathcal{N}(\mathbf{0}, I)$. Noting finally

$$\begin{aligned} \boldsymbol{x} &= \Sigma^{-\frac{1}{2}}\boldsymbol{y}, \\ D &= D_{\Sigma H}N_{D_{\Sigma H}}^{-1} \\ \text{and} \quad \boldsymbol{\theta} &= N_{D_{\Sigma H}}\boldsymbol{\alpha}, \end{aligned}$$

with $N_{D_{\Sigma H}}$ the diagonal matrix composed of the norms of the columns of $D_{\Sigma H}$, we obtain the same model as in Sec. III, that is:

$$\mathcal{H}_1 \ : \ \boldsymbol{x} = D\boldsymbol{\theta} + \boldsymbol{w}.$$

This approach acts in the weighted (by $\Sigma^{-\frac{1}{2}}$) data domain. This allows to implement the detection tests discussed in Sec. III for any target P_{FA}, while including both the specificities of MUSE's instrument (through H) and of the data (through R and Σ). Note that because Σ strongly varies from one spectrum to another, there must be one dictionary D per spectrum.

B. Exploitation of spatial dependencies and analysis of the global FA rate

Two spatially contiguous spectra in MUSE data cubes are likely to share some spectral information, either because the galactic source is resolved (i.e. spread over several pixels), or because of the spatial PSF. The spatial dependencies that exist between neighbors spectra in the hyperspectral data cube can thus be used to increase the detection performances of the considered tests. An efficient detection strategy was proposed in [9], where the spectral information detected in brighter pixels of the data cube is exploited to improve the detection of contiguous faint spectra. This strategy is based on the cascade of two detection tests, as explained hereinafter. After a first detection round using the PDR/LRMAP test on each spectrum of a MUSE data cube (here performed for a $P_{FA} = 0.01 \leftrightarrow \eta = 4.7$), we are left with a set Γ of detected spectra, and a set $\bar{\Gamma}$ of non detected spectra. These two sets are reported, respectively in green and blue, in Fig.4 (center), where the PDR/LRMAP detection results are shown on a MUSE data sub-cube. At this point, a second detection round is performed on all those spectra not detected by the PDR/LRMAP test but contiguous to detected ones. We note these spectra as contained in a subset $\bar{\Gamma}_{\text{f}}$ of

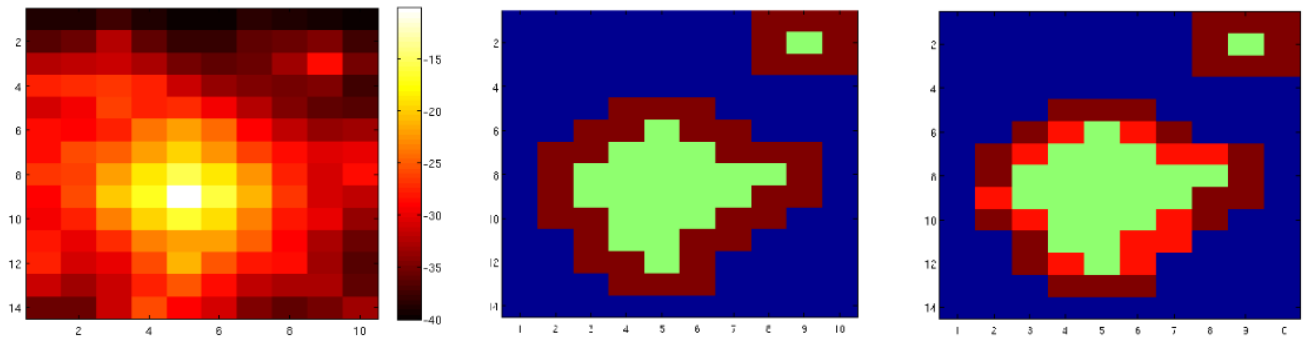

Fig. 4. Part of the simulated MUSE data-cube ($14 \times 10 \times 2048$). Left: SNR map of the considered MUSE sub-cube. Center: spectra where PDR/LRMAP claimed detection at significance level $P_{FA_0} = 0.01$ (Γ set, green) and spectra where LRMPβ is performed (brown). Right: Spectra where LRMPβ claimed detection with a FA rate of 0.01

$\bar{\Gamma}$ (brown pixels in Fig.4 (center)). Denoting by $\boldsymbol{x}_f$ one spectrum in $\bar{\Gamma}_{\mathrm{f}}$ and by $\hat{\boldsymbol{x}}_b$ the estimate (computed by MP) of the $\boldsymbol{x}_f$ brightest neighbor in Γ, the second test we run is the LR-MPβ test, an adapted filter defined as

$$T_{LR-MP\beta} = \frac{p(\boldsymbol{x}_f; \hat{\boldsymbol{x}}_b)}{p(\boldsymbol{x}_f; 0)} \underset{H_0}{\overset{H_1}{\gtrless}} \xi. \tag{20}$$

This test takes account of spatial dependencies between spectra in the data cube, and its $P_{FA} = 2[1 - \Phi(\xi)]$. Supposed to share spectral information with brighter contiguous spectra, $\boldsymbol{x}_f$ is modeled as $\boldsymbol{x}_f = \hat{\boldsymbol{x}}_f + \boldsymbol{w}$, where $\boldsymbol{w} \sim \mathcal{N}(\boldsymbol{0}, I)$ and the estimate $\hat{\boldsymbol{x}}_f$ is computed using the brighter spectrum one ($\hat{\boldsymbol{x}}_b$) (we refer to [9] for further details).

Fig.4 (right) shows the results obtained with the cascade of the two tests. With respect to the case in which only one test is performed, the exploitation of the spatial dependencies between contiguous spectra in the data cube allows to increase the detection performances. Here, thanks to the LR-MPβ test, 12 new detections are added.

The final question to tackle concerns the computation of the overall FA rate. The detection procedure described above cascades two tests: the PDR/LRMAP and the LR-MPβ. For the first test, P_{FA_0} depends only on η while the probability of detection P_{DET_0} depends on η and on the considered spectrum $\boldsymbol{x}_f$. On the other hand, for the LR-MPβ, the probability of FA depends on the ξ threshold, and the detection probability depends on ξ, $\boldsymbol{x}_f$ and $\boldsymbol{x}_b$. Therefore, when cascading the two tests, the overall FA and detection rates are increased with respect to the case where only one test is performed.

Let us consider the case of one spectrum $\boldsymbol{x}_f$ contiguous to one over eight possible bright spectra $\boldsymbol{x}_b$ on a surrounding window of dimensions (3×3). For the two consecutive tests above performed on a spectrum $\boldsymbol{x}_f$, a FA may occur: i) when PDR/LRMAP makes a FA on $\boldsymbol{x}_f$, which happens with probability $P_{FA_0}(\eta)$; ii) when there is no FA by PDR/LRMAP on $\boldsymbol{x}_f$ (probability $(1 - P_{FA_0}(\eta))$), detection of PDR/LRMAP on one of the eight $\boldsymbol{x}_b$ (probability $P_{DET_0}(\boldsymbol{x}_b, \xi)$), and a FA of LR-MP$\beta$ on one of the eight $\boldsymbol{x}_b$ (probability $P_{FA}(\boldsymbol{x}_b, \xi)$). The probability of detection of the two tests is derived similarly, which gives:

$$\begin{cases} P_{FA}^{2tests}(\boldsymbol{x}_f) = P_{FA_0}(\eta) + (1 - P_{FA_0}(\eta)) \times \dfrac{1}{8} \displaystyle\sum_{i=1}^{8} P_{DET_0}(\boldsymbol{x}_{b_i}, \xi) P_{FA}(\boldsymbol{x}_{b_i}, \xi), \\ P_{DET}^{2tests}(\boldsymbol{x}_f) = P_{DET_0}(\eta) + (1 - P_{DET_0}(\eta)) \times \dfrac{1}{8} \displaystyle\sum_{i=1}^{8} P_{DET_0}(\boldsymbol{x}_{b_i}, \xi) P_{DET}(\boldsymbol{x}_{b_i}, \xi). \end{cases} \tag{21}$$

Thus, the P_{FA} increases with respect to the case where only one test is performed but, in any case, we will have that

$$P_{FA}^{2tests} \leq 2 P_{FA_0}. \tag{22}$$

Fig.5 (right) shows the results obtained in terms of FA rate, performing the cascade of the two tests on the MUSE sub-cube considered in Fig.4. The FA rates for spectra tested only once with the PDR/LRMAP test are reported in gradations of blue while spectra tested twice are easily recognizable in red. The FA variation from one spectrum to another is due to the fact that, even if both the PDR/LRMAP and the LR-MPβ tests were set in order to have a $P_{FA} = 0.01$, for the first detection round, according to model (18), one dictionary per spectrum is computed. For a fixed value of the η threshold, corresponding to a mean P_{FA} of 0.01, we thus obtain FA rates which are slightly different, depending on the spectrum we are testing. The P_{FA} map of Fig.3 reports a minimum FA value of $P_{FA_{min}} = 0.008$ and a maximum value equal to $P_{FA_{Max}} = 0.023$. This means that $0.008 \leq P_{FA}^{2tests} \leq 0.023$, which corresponds to a mean P_{FA}^{2tests} of 0.014 over all spectra in the data cube, which is similar to the FA rate set on each detection round, independently.

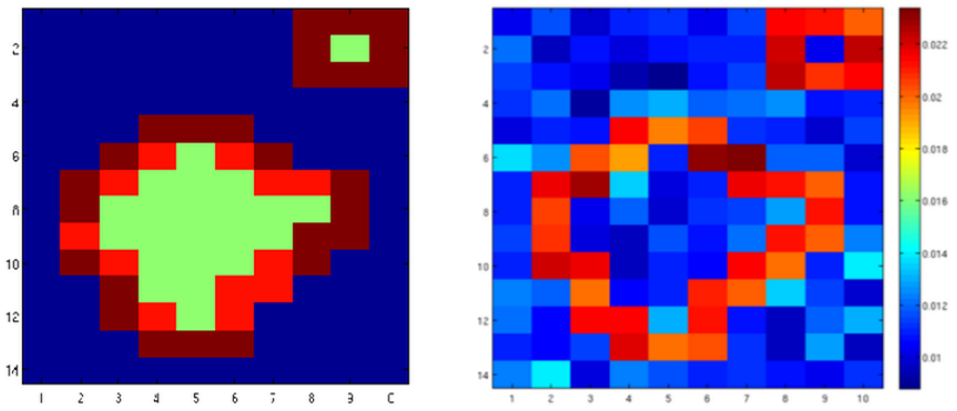

Fig. 5. Resulting P_{FA} map of the simulated MUSE data-cube ($14 \times 10 \times 2048$). Left: Detection results performing the cascade of the two tests. Right: Overall P_{FA} map.

V. Conclusion

Interested in developing new methods for the detection of faint sources drowned in noise, a two steps detection strategy was considered and applied to the astrophysical hyperspectral data of the forthcoming MUSE instrument. This approach cascades two detection tests: the PDR/LRMAP test, which takes advantage from the use of a redundant dictionary, and the LR-MPβ test, aimed to exploit the spatial dependencies existing between contiguous spectra in the data cube. Numerical results on simulated hyperspectral data provided by MUSE consortium, showed an increase of the detection performances with respect to the case in which only one detection test is performed. The analysis of the $P-$values and of the FA rates for the considered tests finally confirmed the reliability of our method, through which improved detection performances were achieved while maintaining the P_{FA} rate reasonably low.

References

[1] E. Arias-Castro, E. J. Candès, and Y. Plan. Global testing under sparse alternatives: ANOVA, multiple comparisons and the higher criticism. *Annals of Statistics*, 39(5):2533–2556, 2010.

[2] S. Basu. Bayesian hypotheses testing using posterior density function. *Statistics and Probability Letters*, 30(1):79–86, 1996.

[3] S. Bourguignon, D. Mary, and E. Slezak. Restoration of astrophysical spectra with sparsity constraints: models and algorithms. *Selected Topics in Signal Processing, IEEE Journal of*, 5:1002 – 1013, September 2011.

[4] S. Chen, D. Donoho, and M. Saunders. Atomic decomposition by basis pursuit. *SIAM Review*, 43(1):129–159, 2001.

[5] D. L. Donoho and J. Jin. Higher criticism for detecting sparse heterogeneous mixtures. *Annals of Statistics*, 32(3):962–994, 2004.

[6] J. J. Fuchs. The generalized likelihood ratio test and the sparse representation approach. In *ICISP'10 Proceedings of the 4th International Conference on Image and Signal Processing*, pages 245–253, 2010.

[7] S. M. Kay. *Fundamentals of Statistical Signal Processing: Detection Theory*, volume 2. Prentice-Hall PTR, 1st edition, 1998.

[8] S. Mallat. *A wavelet tour of signal processing : the sparse way (3rd Edition)*. Academic Press, 3rd edition, 2008.

[9] S. Paris, D. Mary, and A. Ferrari. Pdr and lrmap detection tests applied to massive hyperspectral data. In *Computational Advances in Multi-Sensor Adaptive Processing (CAMSAP), 2011 4th IEEE International Workshop on*, pages 93–96, 2011.

[10] S. Paris, D. Mary, and A. Ferrari. Sparsity-based composite detection tests. Application to astrophysical hyperspectral data. In *19th European Signal Processing Conference (EUSIPCO 2011)*, pages 1909–1913, 2011.